

HOVER TESTING OF A SMALL-SCALE ROTOR WITH ON-BLADE ELEVONS

Rev. 2, 06/10/2000

Mark V. Fulton
Sterling Software, Inc.

and

Robert A. Ormiston
Aeroflightdynamics Directorate
US Army Aviation RD&E Center (ATCOM)

Ames Research Center
Moffett Field, California

Abstract

A two-blade, 7.5-ft diameter dynamic rotor model with 10% chord on-blade elevons driven by piezoceramic bimorph actuators was designed and tested in hover at tip speeds up to 300 ft/sec. The model was designed to maximize elevon actuator performance and succeeded in achieving deflections of ± 5 deg at the nominal rotor speed of 760 RPM. Nonlinear actuator response characteristics were evaluated. Aeroelastic and structural dynamic response characteristics were evaluated over a wide rotor speed range using sine sweep excitation of the elevon up to 100 Hz. The CIPHER[®] post processing method was very useful for determining frequency response magnitude and phase of measured blade root flap bending and torsion moments to elevon input and elevon response to actuator input voltage. Preliminary experimental results include actuator effectiveness, effects of low Reynolds number on elevon pitch moments, elevon control reversal, and variation of flap bending mode responses with rotor speed and elevon excitation. The model performed satisfactorily and the results provide an encouraging basis for future wind tunnel testing that will evaluate on-blade elevon effectiveness for reducing rotor blade vibratory loads.

Introduction

There has long been a desire to reduce helicopter vibration. Traditional approaches are based on optimizing the rotor and fuselage structure to minimize response to unsteady aerodynamic excitation, or installing vibration absorbers or isolators in the rotor or fuselage. In recent years increasing attention has been devoted to active higher harmonic control of blade root pitch to reduce vibration at the source. The early work by McHugh and Shaw (Ref. 1) and other investigators used higher

harmonic control (HHC) swashplate inputs to drive blade root pitch to attenuate vibratory loads. This technique was very successful in reducing fixed system vibratory loads, but actuator power at high flight speeds and fail safety considerations have tempered interest in this approach (Ref. 2). Efforts are continuing, however, to apply HHC and individual blade control (IBC) to benefit rotorcraft performance, vibration, and BVI noise, e.g. Refs. 3 and 4.

The inherent problem in blade root pitch active control is pitching the entire blade at multiples of the rotor rotation frequency. As an alternative, considerable effort is now being directed toward more localized on-blade aerodynamic control concepts. Combined with newly emerging actuation capabilities of smart materials (see Refs. 5-8), these approaches hold considerable promise for future advanced rotors. There are two principal methods of implementing such concepts: 1) incorporation of smart materials into the blade structure to control the local twist of the blade - active twist, and 2) actuating a trailing edge control surface, or elevon, to generate local aerodynamic lift and pitch moment - active elevon. The latter concept is an adaptation of the Kaman servo-flap control system and the multi-cyclic controllable twist rotor concept (MCTR), Ref. 9. An advantage of the active elevon concept is that multiple elevons per blade may be introduced, providing additional independent controls to attenuate additional components of vibratory loads. Although the force and displacement capabilities of smart materials are limited at the present time, a future implementation of the active elevon concept might provide flight control functions of the rotor, eliminating the conventional actuators, swashplate, and blade pitch links. Such an idealized configuration (Ref. 10), shown schematically in Fig. 1, would also integrate the actuator material into the blade structure, replacing the discrete, hinged, elevon with a continuously curved surface at the trailing edge of the airfoil, eliminating mechanical linkages and

components further improving maintenance and reliability.

Although various terms have been used for rotor on-blade control surfaces, such as flap, aileron, servo-flap, etc., the term elevon is used herein to distinguish it from other meanings commonly associated with these devices. For example, flap is used for a high-lift device, and for rotor blade motion in the flap direction; aileron is used for a roll control surface; and the Kaman servo-flap is the airfoil used to control rotor blade collective and cyclic pitch.

Analytical investigations by Millott and Friedmann, Refs. 11 and 12, and Milgram and Chopra, Ref. 13, have shown that the active elevon control concept is theoretically practical for reducing rotor vibratory forces and moments transmitted to the fixed system, that is, with one elevon per blade, and for practical deflection amplitudes, vibration reduction is comparable to HHC blade pitch. Moreover, the elevon actuator power is significantly less than the HHC power required to pitch the entire blade. These studies also included preliminary investigation of optimizing the structural dynamic properties of the blade such as torsion frequency placement and elevon location.

A number of preliminary design studies have also been conducted to explore the practical feasibility of designing full-scale rotor systems with smart material actuators and/or active elevons for reducing rotor vibration and, in some cases, providing rotor flight control. (Refs. 14-16)

In recent years a number of efforts have been initiated to investigate and experimentally demonstrate the capabilities of active on-blade control surfaces, primarily using small-scale rotor models in conjunction with smart material actuators. One of the earliest experimental investigations by Spangler and Hall, Ref. 17, used a simple 6.25-in chord, 2-D wing with a piezoceramic bimorph actuator driving a 10%-chord trailing edge flap. At a wind tunnel velocity of 78 ft/sec, flap deflections of 12 deg were achieved with an electric field of 8.8 V/mil, 4 Hz excitation. At the low Reynolds Number of 2×10^5 , lift and pitch moment were substantially lower than predicted by thin airfoil theory. Early rotor system experiments were reported by Chen, Samak, and Chopra, Refs. 18 and 19. Wind tunnel testing of a piezoceramic bimorph-driven 4.25-in span, 20% chord flap on a 3-in chord blade achieved 7 deg deflections at 110 ft/sec velocity with 5 V/mil, 5 Hz excitation. Rotor testing in hover (four blades, 6-ft diameter) achieved 8 deg elevon deflection at 300 RPM for 1-4/rev excitation at 5 V/mil. Elevon deflection decreased to 1.5 deg (averaged over 1-4/rev) at 900 RPM as a result of

aerodynamic hinge moments and centrifugal force effects on the elevon, bearings, and linkage mechanisms.

Improvements in the design of the bimorphs and linkage mechanisms, Ref. 20, suggested elevon deflections could be improved but this was not demonstrated in subsequent testing, Ref. 21. Still further improvements, including additional bimorph layers, optimizing elevon and actuator characteristics, and improved elevon bearings to support centrifugal loading reported by Ben-Zeev and Chopra (Ref. 21) were successful in improving elevon deflection. A single bimorph, 1.5-in span elevon, at 95 V rms and 50 Hz achieved 13 deg at 300 RPM and 4 deg at 750 RPM before decreasing abruptly to 0.5 deg at 900 RPM.

These results serve to clearly illustrate the technical challenges of generating adequate elevon deflections in small-scale model rotors, completely aside from other important aeroelastic and structural dynamic issues that may arise when the active elevon concept is applied in a practical system to reduce rotorcraft vibratory loads.

A few practical questions might include the following. For example, what bending and torsion frequency placements are favorable? How does elevon effectiveness vary with rotor speed and excitation frequency and what are the effects of forward flight on dynamic response? What aeroelastic coupling characteristics result from a blade control device operating in the rotating system? What is the relative importance of lift and moment of the elevon and what are the mechanisms by which the lift and moment influence vibratory airloads and loads (lift effect and torsion effect)? How are these mechanisms influenced by rotor speed, excitation frequency, and blade frequency placement? What is the effect of the flap bending mode shapes on these mechanisms? Such questions will need to be answered before active elevon blade control can be intelligently applied to design optimum rotor systems to relieve vibratory blade and hub loads of lifting rotors in forward flight.

The present investigation was initiated to address some of the difficulties of developing a small-scale active-elevon rotor with piezoceramic bimorph actuators, and demonstrate the ability to generate useful elevon deflections in hover. Other objectives were to explore fundamental aeroelastic, structural dynamic, and dynamic response characteristics of a rotor blade to elevon control excitations as noted above.

The scope of the present investigation is limited to a unique, two-blade, hingeless rotor configuration tested at low tip speeds and low to moderate thrust

coefficient. Although not dynamically representative of full scale rotor systems in all respects, the model dynamic characteristics are sufficiently representative to permit investigation of many aspects of full scale systems. The emphasis is on fundamental structural dynamics characteristics; investigation of rotor performance and important nonlinear aerodynamic stall and compressibility effects will require a more sophisticated rotor. The model was not equipped with a closed loop vibration control system - all excitations were open loop. Minimal instrumentation was installed, and primary measurements were confined to elevon deflection and blade root bending and torsion moments. The paper will address the design and development of the model rotor blades, including the piezoceramic actuators and elevons, and then present quasi-steady and dynamic test data for nonrotating and rotating conditions in hover. Results of forward flight wind tunnel testing will be presented at a future time.

Optimum Elevon and Actuator Design

An analytical design study was undertaken to better understand the factors influencing active rotor design. For a brief description, see Ref. 22. The goal was to develop a configuration that would maximize the aerodynamic effectiveness for a given amount of actuator material for a specified airspeed. The design, of course, was also subject to the practical constraints of a small-scale model. Various structural configurations were investigated, including distributed blade twist, deformable trailing edge tabs, and discretely hinged elevons. For the hinged elevon design, several actuation concepts were explored. Finally, several different active (or "smart") materials were investigated before choosing piezoceramic material. Piezoceramic materials were found to have a good combination of induced strain, stiffness, and response time for the present study. For a complete and excellent review of active rotor design considerations, see Ref. 5.

In brief, the choice of a discretely hinged elevon was driven by the small strains typically available from current active materials. Use of a stack actuator required the leveraging of the resultant motion into a range suitable for elevon deflection. For the small scale rotor envisioned, such amplification seemed difficult to create. The natural benefit of the bimorph configuration (Fig 2) is that amplification is built into the actuator in that the strains of the upper and lower piezoceramic layers cause a vertical deflection of the beam's tip which is much larger than the total deformation of either PZT layer. The trade-off, of course, is that the blocked force is much lower than that of stack actuators. The blocked force, however, matches well with the requirements of elevon

actuation as long as the actuator stiffness is matched with the load stiffness (the aerodynamic "spring" stiffness). (See Ref. 17 for a detailed discussion of the governing equations.)

As noted in the introduction, though, previous small-scale rotor models have not achieved desired trailing edge control deflections when operating at moderate and higher rotor speeds and subject to aerodynamic forces. Possible causes include: 1) sub-optimum design matching of actuator stiffness to elevon aerodynamic stiffness, and 2) mechanical design problems with the elevon installation and actuator linkage mechanism. The optimum design problem is now addressed.

The piezoceramic, lead zirconate titanate (PZT), bimorph bender beam is cantilevered to the rear of the rotor blade main spar. A lever arm projects forward from the elevon to engage the tip of the cantilever PZT beam to produce elevon rotational motion, conceptually shown in Fig 2. In studying this particular configuration, the design space was first investigated generically. Bernoulli-Euler beam theory was used, along with the assumptions of perfect bimorph bonds, and quasi-static, 2-D linear airfoil theory. A PZT material was chosen, along with a PZT to elevon width ratio, and an airspeed. Then the PZT thickness and lever arm length were varied. For illustration purposes, the resultant elevon deflection is plotted against these two variables in Fig 3. This figure shows that for any PZT thickness an optimum lever arm exists which matches the bimorph stiffness with the aerodynamic stiffness. Note that in Fig 3 the PZT thickness is normalized by the maximum elevon thickness and the lever arm length is normalized by the elevon chord. The normalization of the PZT thickness is particularly significant in that it indicates the geometric constraint of the airfoil cavity.

Based on the encouraging results from this generic study, a design for a small-scale rotor was initiated. For this concept, it was believed that a 10% chord elevon with an amplitude of motion of 5 deg would yield sufficiently large control authority to perform an exploratory hover test. A design plot was therefore created for an available bimorph under the constraint of the available chord-wise space for the actuator. The bimorph to elevon width ratio was specified to be 0.54. The design velocity was 270 ft/sec and two aerodynamic spring stiffnesses were chosen: a nominal stiffness based on an elevon hinge moment coefficient ($c_{h\delta} = 0.44/\text{rad}$) and a value increased by a factor of 1.5. Figure 4 shows the elevon deflection as a function of bimorph length. This plot assumes that the root of the bimorph is clamped to the aft side of the spar. Only one length, then, gives the optimum lever arm, thereby maximizing the elevon deflection. This

plot showed that a free bimorph length of 1.8 inches would be optimum. Note that the design specification of 5 deg was satisfied using an excitation voltage of 90 V (12 V/mil) and assuming a piezoelectric strain coefficient d_{31} of 7.09×10^{-6} mil/V. (To first order, the actuation strain, Λ , equals d_{31} times the applied electric field.) It was believed, however, that an oscillatory voltage up to 156 V (20.7 V/mil or 110 Vrms) could be used in the experiment without fatiguing the PZT, with the excess voltage being available for lost motion due to hysteresis, friction, aerodynamic damping, slop, or any other unmodeled effects.

These design predictions suggested that relatively large elevon deflections (10 deg nonrotating and 5 deg at operating speed) could be achieved at the anticipated operating conditions. The predicted variation of elevon angle with velocity is shown in Fig 5. As before, this prediction assumes an excitation voltage of 90 V (12 V/mil). Quasi-static, 2-D linear airfoil theory was used and all rotor speed effects (such as mechanical friction) were neglected.

The desired bimorphs were purchased from Piezo Systems, Inc. and were trimmed in size from the Standard 2-Layer Piezoelectric Motor Element T220-A2-501. The standard width of 1.5 in was retained but the length was reduced to 2.05 in (including 0.25 in for clamping). These bimorphs are made from two piezoceramic 5A layers, each 0.0075 in thick, bonded on either side of a metallic center shim. The combined thickness is 0.020 in. The bimorphs were poled for parallel configuration and had nickel electrodes. A semicircular hole was ground at the edge of the upper 5A layer to permit access to the center shim. This actuator was specified by the manufacturer to provide a blocked force of 1.6 oz and a free deflection of ± 0.048 in for a free length of 2 in when ± 180 VDC (12 V/mil) is applied.

Experimental Model Development

For the objectives of a preliminary investigation to explore fundamental behavior, a low tip speed, small-scale dynamic model was acceptable and reduced cost and complexity. In order to further reduce model development time and cost, it was decided to modify two prototype blades from an existing 7.5-ft diameter Mach-scaled, low torsion stiffness hingeless rotor model designed and built for a previous research project. Blade structure was removed behind the main spar to install an elevon and piezoceramic bimorph actuators at the 0.75R location. The removal of load-carrying structure to accommodate the elevon and actuators apparently reduced the active section strength, suggesting a reduced rotor speed. Of more significance, however, was the fact that a reduced tip speed was required to enable useful elevon motions

with the available actuator power. Even at 760 RPM, however, the dimensionless torsional frequency remained acceptable due to the original low torsional stiffness. At the reduced tip speed (298 ft/sec) the low tip Reynolds number (5.4×10^5) would be expected to affect airfoil drag and stall behavior. These effects, however, are not large and the compromise is acceptable for the predominantly low thrust dynamic response characteristics of interest here.

The rotor blades are untwisted, straight, hingeless blades of uniform mass and stiffness except at the blade root and the elevon "active section". Chordwise mass and aerodynamic center are located near the quarter chord point of the symmetrical NACA 0012 airfoil section. The blades are constructed of composite materials including a fiberglass spar, foam filled core, and fiberglass wrapped skin construction. Additional construction details for the similar blades tested by Maier et al. are available in Ref. 23. Substantial discontinuities in the blade mass and stiffness occur near the active section. The general characteristics and properties of the rotor system and blades are given in Table 1.

Elevon-Actuator Aerodynamic and Mechanical Design

As noted earlier, the second possible cause of poor actuator and elevon deflection performance is mechanical design problems with the elevon installation and actuator linkage mechanism. This problem will now be addressed. Mechanical sources of diminished elevon deflection performance include a variety of possible causes - aerodynamic hinge moment, centrifugal inertial (tennis racket) effect, pivot bearing friction arising from flap centrifugal forces, and friction and binding of actuator and elevon linkage mechanisms. The design of the present model was undertaken with the aim of minimizing these effects insofar as possible in order to maximize the elevon deflection.

In order to minimize possible loss of elevon deflection from mechanical problems, considerable attention was devoted to the design and construction of the elevon hinge and lever mechanism. This involved minimizing unwanted friction forces and free play in the elevon linkage mechanism. These two effects are not independent, since free play can be reduced by tightening tolerances but this can increase friction or possibly even binding of the mechanism. The present design approach emphasizes several key areas, and is illustrated in Fig 6 with an airfoil cross section at the elevon and actuator location. To reduce friction, steel pins bonded to the ends of the PZT bender beams engaged elevon lever arms made of fiberglass. Slots in the lever arms accommodated

small translations of the bender beam pins necessitated by the opposing arc motion of the two components; a slot size equal to the pin diameter was used to minimize free play and friction at the same time. Most importantly, the steel elevon hinge pins were mounted in low friction Delrin bearing blocks attached to the blade, with a brass and Teflon thrust washer pair used to support the elevon centrifugal force exerted against the outboard Delrin hinge pin bearing blocks. Finally, adjustments were made to the alignment of all contacting components, including the PZT bender beam pins, the elevon lever arms, the elevon pivot pins, and the bearing blocks, to minimize friction and binding.

The planform design of the elevon and actuator installation included two PZT bimorph actuators driving a single elevon (Fig 7). The design used a 10% chord plain elevon with a span of 12% blade radius, centered at the 75% radial location. The elevon was hinged only at the ends in order to simplify fabrication and to reduce the chance of mechanical binding. The 10% chord elevon was believed to be the smallest chord size which could be fabricated and still provide good aerodynamic effectiveness. This choice also yielded a practical lever arm distance and allowed the use of commercially available PZT bimorph materials. The 75% radial location was not specifically chosen to maximize response of any particular flap bending mode, rather it was simply chosen as a suitable representative location for exploratory testing.

The modifications to the original blade structure to accommodate the actuator and elevon required removal of the upper surface fiberglass skin and foam core filler material behind the main spar as well as the lower surface skin at the elevon trailing edge location; see photo of blade section in Fig 8. Two epoxy and chopped glass ribs were bonded between the skins at the boundary of the cutout section with a third midway between the two PZT actuators. The outer ribs provide attachment for the Delrin bearing blocks and provide a load bearing surface for the removable upper surface hatch. This hatch was secured to the three ribs with flush mounting screws. The PZT actuator bimorphs were clamped between an upper fiberglass block and a lower aluminum bolt block. The lower blocks were in turn bolted to the fiberglass main spar. Finally, access holes were cut in the upper skin in front of the spar for the insertion of ballast weights to maintain quarter chord mass balance in the elevon region of the blade. The holes also allowed access for installing nuts for the spar bolts.

As will be shown, the two blades exhibited somewhat different characteristics. The primary differences appear to be related to bimorph actuation effectiveness and elevon aerodynamic effectiveness.

The exact cause of these differences is not known, but they are believed to be caused by differences in the structural characteristics of the bimorph/elevon configurations as well as active section airfoil contour variations from blade to blade.

Electrical Excitation

The bimorphs in each blade were electrically connected in parallel. Each resultant bimorph pair was powered by a Trek Model 50/750 High Voltage, Solid-State Amplifier. The AC command voltage given to the Trek was from a function synthesizer. This voltage was either a single frequency (between 5 and 100 Hz) or a logarithmic frequency sweep (from 1 to 105 Hz). The AC voltage never exceeded 110 Vrms. This AC voltage was superimposed on a DC voltage used to bias the bimorph layers in the direction of their polarization to avoid depolarization by the relatively large AC voltage. Each bimorph pair was powered through a separate Trek channel, but both channels were provided with the same AC voltage command. At times, one blade was given a different DC bias in order to help compensate for blade to blade differences in mean elevon position. The center shim of each bimorph pair had a 5 k Ω resistor in series to provide surge protection during atypical operation. This resistor, of course, would absorb more and more voltage as the frequency was increased since the capacitive-like PZT would draw more current at higher frequencies. For fixed frequency testing, the command voltage was adjusted to the required level. For the logarithmic frequency sweeps, the command voltage was set to a desirable level at a low frequency, and the PZT voltage would be allowed to drop as the frequency increased.

Rotor and Test Stand

The hover testing was conducted in the AFDD Hover Test Chamber with the Small Scale Rotor Test Rig (RTR). The control console was used to input the required collective pitch. The stand balance system was locked out and not used; no fixed system rotor forces were measured. The existing RTR slip ring was used for instrumentation and an additional slip ring was installed above the rotor hub for supplying electrical power to the PZT actuators. A photograph of the RTR and rotor system installed in the hover test chamber is shown in Fig. 9.

Instrumentation, Data Acquisition, and Processing

Elevon motion was measured with a Hall-effect transducer. The accompanying magnet was poled through its diameter and was bonded to the inboard elevon bearing pin to rotate with the elevon. Blade response was measured through full strain gage

bridges at the root flexure of each blade. The flap and chord strain gage bridges were at 0.114 R, and the torsion strain gage was at 0.128 R. In addition, the pitch of blade 1 was measured with a potentiometer. Both PZT voltage and current were measured.

The PZT power was routed from the hub to the active section on the exterior of the blade, near the quarter chord. The power and signal for the elevon Hall-effect transducer was routed from the hub to the active section on the exterior of the blade, 0.5 in forward of the trailing edge.

Analog six-pole Bessel filters were used with a -3 dB cut-off frequency of 100 Hz. All of the transducers were discretely sampled and digitized. Unless otherwise noted, the dynamic data was acquired at a sample rate of 543 Hz. Dwell tests were sampled for 7.5 sec while logarithmic frequency sweeps were sampled for 30 sec.

For the dwell tests, analysis of the acquired time histories was performed using an in-house analysis. This program was used to display the time histories, extract their means, and obtain the frequency content using a Fast Fourier Transform (FFT).

For the frequency sweeps, frequency response functions (FRF's) were obtained using CIPHER[®] (Comprehensive Identification from Frequency Responses), Refs 25 and 26. The CIPHER[®] program FRESPID (Frequency RESPONSE IDentification) was used to obtain the FRF's for five different window lengths. FRESPID concatenated two 30 sec time histories for each of the reported rotating cases. For some nonrotating cases, however, only one time history was used. FRESPID performed final signal conditioning by use of a digital filter with a -3 dB cut-off frequency of 105 Hz. Finally, the CIPHER[®] program COMPOSITE was used to perform multi-window averaging of the FRESPID results. These COMPOSITE results are reported in this paper.

The CIPHER[®] results are presented for either individual blades or for average responses (not to be confused with window averaging). The average responses were calculated by averaging the time histories from the two different blades to obtain the response of an "average" blade. These averaged results were then processed by CIPHER[®].

Fan Plot Description

The fan plot of rotor blade frequencies in the rotating system are shown in Fig 10 as a function of rotor speed in air at zero deg collective pitch. The nominal operating speed is 760 RPM (12.7 Hz). These

frequencies are analytical predictions of the Second Generation Comprehensive Helicopter Analysis System (2GCHAS) using blade properties adjusted to match measured frequencies at zero rotor speed. The measured nonrotating blade frequencies were found to be 3.66, 12.0, and 55.6 Hz for flap, chord, and torsion, respectively. The nominal rotor speed results in a representative first-flap frequency (1.11/rev). The rotor is stiff inplane, having a first lead-lag frequency just above 1/rev at 1.08/rev. Although not of direct consequence for the principal elevon-flap-torsion response characteristics of interest, this makes the rotor sensitive to chord loads from aerodynamic 1/rev and cyclic flapping excitation. The nominal rotor speed also results in a second flap bending mode above 3/rev unlike most blades, where this mode is below 3/rev. The combination of low torsion stiffness and low rotor speed results in a reasonable first torsion frequency of 4.6/rev. Both the first elevon/actuator and third flap bending frequencies are between 6/rev and 7/rev at nominal rotor speed. A pretest prediction of the bimorph/elevon fundamental natural frequency was made assuming quasi-static 2-D airfoil conditions and ignoring mechanical friction. The frequency was predicted to be 80 Hz for zero airspeed and to increase slightly with RPM.

The fan plot shows the variation of the natural frequencies with rotor speed. For the purposes of the present investigation, varying the rotor speed provides a powerful means of exploring the dynamic response characteristics of the rotor blades when excited by the elevon.

Experimental Testing and Results

Much of the testing occurred at the nominal rotor speed of 760 RPM, although results are also reported for 0, 200, and 425 RPM. All results in the paper are restricted to approximately zero cyclic pitch; that is, no attempt was made to minimize the 1/rev flapping. The collective pitch is 3.5 deg unless otherwise stated. For collective sweeps, a total range of -6 to +6 deg is reported. Elevon motion tests were performed using dwell tests (5-100 Hz) or logarithmic elevon frequency sweeps (1-105 Hz in 27 sec). Quasi-steady data (approximating steady-state results) was taken at a low frequency of 5 Hz to facilitate data acquisition and to minimize the effects of static friction and instrumentation zero drift. At 5 Hz the torsion response remains essentially steady state. In some cases, the voltage level was varied to investigate nonlinearities. The maximum AC voltage applied was 110 Vrms.

The results of experimental testing will be presented in sequence, first examining the static, or

quasi-steady (low frequency elevon excitation) characteristics of the system, for first the nonrotating and then the rotating condition. Next, the actuator effectiveness, elevon effectiveness, torsion aeroelastic response, and flap bending aeroelastic response will be examined. Finally, dynamic response results will be presented to address the system characteristics, both nonrotating and rotating, for the full range of elevon excitation frequency.

Quasi-Steady Results

Actuator Effectiveness, Nonrotating

The basic mechanical and electrical characteristics of the elevon and PZT actuators are first examined. The piezoceramic material is characterized by significant nonlinear behavior and this can be observed in the basic static and dynamic response characteristics of the elevon system. Figure 11 shows steady state elevon deflection for a full cycle of increasing and decreasing excitation voltage showing a characteristic hysteresis loop. A more relevant characterization is elevon deflection versus excitation voltage for a low frequency periodic excitation. In Fig 12, the elevon amplitude (1/2 PTP) is shown as a function of the excitation voltage at 5 Hz frequency. There is a threshold excitation before elevon deflection is produced and the maximum elevon deflection is limited by interference of the lever arm against the interior of the airfoil skin surface at approximately ± 10 deg. Figure 12 also includes the variation in the mean elevon deflection as a function of excitation voltage.

Sample elevon deflection time histories are shown in Fig 13 for several values of excitation voltage in order to more clearly illustrate the nonlinear behavior. For the low frequency 5 Hz cases, the PZT actuator nonlinearity is evident at low excitation voltage and the elevon waveform is clipped by mechanical interference at the maximum deflections.

For completeness, this section will include a discussion of the dynamic response of the nonrotating elevon/actuator combination obtained using the CIPHER[®] method. Figure 15 shows the frequency response functions for the elevon deflection and the PZT current. The elevon dynamic response strongly reflects the mechanical dynamics of the system and reveals a resonant response peak near 80 Hz, which is the elevon/PZT beam first natural frequency. Note how the corresponding electrical admittance (mA/V) is not a linear function of frequency as a pure capacitor would be. In fact, the local minimum reveals the electromechanical coupling of this piezoceramic actuator. (See Ref. 27 for further information.) As anticipated, the elevon/PZT fundamental frequency

(near 80 Hz) was sufficiently above the harmonics of primary interest that it did not play an important role during hover testing. Even if this were not the case, a future section will demonstrate that this resonant amplification of the elevon deflection is eliminated as 760 RPM is approached.

Actuator Effectiveness, Rotating

The basic measure of the effectiveness of the PZT actuator-elevon system is the ability of the actuator to produce required elevon deflections with full centrifugal and aerodynamic forces present. Rotating tests of the present design showed that elevon deflection performance was quite good. Typical results for elevon deflection over a range of operating rotor speeds are shown in Fig 16 for several levels of RMS excitation voltage. At the nominal 110 Vrms PZT excitation, elevon deflections of more than ± 6 deg were achieved at the nominal rotor speed of 760 RPM.

The results in Fig 16 show a gradual decrease in elevon deflection with rotor speed as a result of the increasing aerodynamic elevon hinge moment, and this trend is consistent with the behavior expected by original design predictions - elevon angle varying in proportion to $1/(1 + KV^2)$. There is no evidence of mechanical binding of the actuator or elevon linkage mechanism. As shown in Fig 16, the low voltage PZT excitation was applied over the full rotor speed range with elevon deflection approaching mechanical constraint of airfoil contour geometry at low rotor speed. For this reason, the application of higher voltage PZT excitation was restricted to higher rotor speeds and thus elevon deflections are not shown in Fig 16 for combinations of low rotor speed and high voltage.

Although substantial elevon deflections were achieved, they are somewhat less than anticipated for a given excitation voltage level. A result for 64 Vrms excitation based on the actuator-elevon design prediction is included in Fig 16. The difference suggests that elevon bearing friction, aerodynamic damping, and hysteresis reduced the predicted motion. These unmodeled effects were taken into account by reducing the maximum voltage in the theoretical prediction. For this reason, the elevon deflections are considered satisfactory for present purposes. It may also be noted that the elevon performance differs between the two blades; it is presumed that aerodynamic, electro-mechanical, and friction differences between the two elevons and PZT bender beams are responsible. Other possibilities include sensitivity at low Reynolds number to airfoil contours of the actuator access panels and variations of the external instrumentation leads.

A cross plot of elevon deflection performance versus excitation voltage is shown in Fig 17 for 5 Hz excitation at 760 RPM. The “dead band” region is evident at low excitation voltage due to PZT hysteresis noted earlier but here it is less prominent than in the nonrotating case, Fig 12.

When operated at non-zero collective pitch, static response is subject to elevon floating characteristics ($c_{h\alpha}$ hinge moment derivative). The floating response is governed by the relative strength of the steady aerodynamic hinge moment and the stiffness of the PZT bender beam. This is evident in the mean or average elevon deflection as rotor blade collective pitch is varied. Typical results are shown in Fig 18, for 5 Hz excitation at 760 RPM. Again, there are differences between the two blades but the expected trend is observed, that is, for increasing collective pitch, the elevon floats in the trailing edge up direction.

Elevon Effectiveness and Torsion Moment Aeroelastic Response

Given that a PZT actuator is successful in producing sufficient elevon deflection, it is of interest to examine the effectiveness of the elevon in producing blade aerodynamic lift and pitching moments. We will first examine the pitching moment effectiveness of the elevon. For untwisted blades, at low collective pitch, the blade root elastic torsion moment measurements directly reflect the blade aerodynamic pitching moment resulting from elevon deflection since the elevon pitching moment is reacted only by the torsional rigidity of the blade and the torsional inertial stiffness (tennis racket effect) of the blade.

The measured torsion moment response versus the elevon deflection amplitude for 5 Hz excitation at 760 RPM is shown in Fig 19. Note that the results are linear for both blades except at small elevon deflections, where again there are substantial differences between blades. These differences most likely reflect elevon and airfoil contour differences of the two elevons. If the moment response is normalized by the corresponding elevon amplitude, a measure of torsion/elevon aeroelastic response effectiveness is obtained.

The normalized torsion moments for both blades are plotted as a function of rotor speed in Fig 20 and show quadratic behavior reflecting an elevon aerodynamic pitch moment proportional to dynamic pressure. At higher rotor speeds, the tennis racket effect increases, and the torsion response moderates. This moderation, however, is not pronounced for the range of rotor speeds tested.

Compared with expected elevon performance estimates, the measured elevon effectiveness in Fig 20 is significantly lower than had been anticipated based on the thin airfoil theory. To briefly illustrate, a simple approximate expression for static torsion response is developed as follows.

$$\begin{aligned} M_{\text{aero}} &= qSC c_{m\delta} \delta \\ &= K_{\phi}\phi + I_{\phi}\Omega^2\phi \end{aligned} \quad (1)$$

Solving these equations for the torsion response of the blade yields

$$\phi/\delta = qSC c_{m\delta} / (K_{\phi} + I_{\phi} \Omega^2) \quad (2)$$

$$M_{\phi} / \delta = (\phi/\delta)K_{\phi} \quad (3)$$

Using approximate lumped parameter values representative of the elastic blade properties, an analytical estimate for the blade torsion moment is

obtained using the thin airfoil theory value for $c_{m\delta}$ (0.55/rad for a 10% chord plain flap). The result is included in Fig 20 and is seen to significantly exceed the measured results.

The reason for the difference is presumed to be due, in part, to the effects of the low Reynolds number $\sim 4.0 \times 10^5$ at the blade elevon radial position. It is well known that airfoil lift characteristics at low angles of attack are moderately influenced at such low Re, but there is very little data available for airfoil pitch moment of trailing edge flaps at such low Re. Limited data for a 12.5% symmetrical RAF 30 airfoil (Ref 24) at 3.6×10^5 Re suggests that the aerodynamic pitch moment response to trailing edge flap deflection is about 60% of the amount expected on the basis of inviscid thin airfoil theory. Using a value for $c_{m\delta} = 0.34/\text{rad}$ yields an improvement in Fig 20, however the measured results are still overpredicted.

In an attempt to further explore the possible influence of low Re on the elevon aero pitch moment characteristics, modifications to the elevon shape were undertaken. These modifications included thickening the trailing edge analogous to a Gurney flap, sealing the elevon-to-blade hinge gap, and increasing the trailing edge angle by adding a series of progressively thicker wedges to increase the thickness at the trailing edge of the elevon. The latter shape alterations did increase the elevon aerodynamic effectiveness by up to 59%. Such major shape alterations are not proposed as practical means of improving elevon effectiveness, but were investigated to explore a simple means of

offsetting a possible drawback of testing at low Re conditions.

It is of interest to describe elevon effectiveness in terms of the associated tip torsion deflection (note that for practical applications, this implies that the elevon would be designed to exploit the “torsion mode” of operation rather than the “lift mode” as discussed in the next section). For the present model, Eq 2 yields $\phi/\delta = 0.072$ using the theoretical elevon derivative $C_{m\delta} = 0.55/\text{rad}$. For a 5 deg elevon deflection, this yields $\phi = 0.36$ deg tip torsion deflection. At the torsion mode natural frequency, the amplitude is increased by roughly a factor of five (see discussion below) thus the maximum torsion deflection would be $\phi \sim 1.8$ deg. Note, however, these are ideal values and the elevon effectiveness of the present small scale model was considerably reduced for the reasons discussed above.

The effect of rotor blade collective pitch on elevon effectiveness was investigated and results are shown in Fig 21 for the 5 Hz excitation at 760 RPM. The elevon effectiveness decreased slightly with positive collective pitch up to 6 deg for blade 2, and decreased for both blades for negative collective pitch angles up to -6 deg. The reduction evident at zero collective pitch is likely due the blades operating in each other’s wake. Both the elevon amplitude and torsion moment decreased substantially for negative collective pitch angles; the relatively larger decrease in the torsion moment resulted in the decrease in the normalized elevon effectiveness.

Flap Bending Aeroelastic Response, "Elevon Reversal"

Analogous to “steady state” elevon-torsion effectiveness arising from the aerodynamic pitching moment of the elevon, it is of interest to examine the corresponding flap elevon-bending effectiveness arising from the aerodynamic lift of the elevon. This is determined from measurement of flap bending at the blade root. However, in this case, the torsion effect of the elevon must be accounted for and the concept of flap bending elevon effectiveness becomes more complex. This is because, in addition to the blade lift produced directly from elevon deflection ($C_{l\delta}$), an opposing blade lift is also indirectly produced from elastic torsion (angle of attack, $C_{l\alpha}$) caused by the elevon pitching moment.

Results for blade root flap bending normalized by the measured elevon deflection for the 5 Hz “quasi-steady” excitation frequency are shown in Fig 22 as a function of rotor speed. Interestingly, the variation is roughly quadratic at low rotor speed, but approaches a peak value at approximately 450 RPM before

diminishing to near zero at the 760 RPM nominal rotor speed. It is evident that the direct aerodynamic lift of the elevon is being overcome by the indirect blade twist induced by elevon pitch moment as the rotor speed increases, leading to what is termed “elevon reversal” near 760 RPM. (Note that an actual reversal in flap bending was not observed at 760 RPM but would be expected at a slightly higher rotor speed.) This phenomenon is analogous to fixed wing aircraft aileron (roll control) reversal caused by insufficient wing torsional rigidity at high flight speed.

The “elevon reversal” phenomenon may be illustrated by using a simplified rigid, hinged, spring restrained, rotor blade to model the first bending and torsion modes of a cantilever hingeless blade. The aerodynamic lift and moment of the elevon are taken to act at the midpoint of the elevon portion of the blade and the distribution of lift arising from blade torsion is accounted for by the parameter K_α . Choosing inertia and stiffness values to approximate the elastic physical model, simple expressions may be used to help confirm experimentally measured behavior. The applicable equations may be written as follows:

$$\begin{aligned} M_{\beta\text{aero}} &= qRS(C_{l\delta} \delta + K_\alpha C_{l\alpha} \alpha) \\ &= K_\beta \beta + I_\beta \Omega^2 \beta \end{aligned} \quad (4)$$

Substituting $\alpha = \phi$ and using the previous expression for torsion angle, Eq 2, the solution for the flap bending response becomes:

$$\beta/\delta = qRS(C_{l\delta} - K_\alpha C_{l\alpha} C_{m\delta} qSc / (K_\phi + I_\phi \Omega^2)) / (K_\beta + I_\beta \Omega^2) \quad (5)$$

$$M_\beta / \delta = (\beta/\delta)K_\beta \quad (6)$$

These expressions clearly show the fundamental behavior of the flap bending response and influence of the pertinent aerodynamic and structural parameters of the rotor blade. It may be seen that as dynamic pressure (q) increases with rotor speed, there will be a point where M_β / δ will reverse sign. Equation 6 was used to calculate representative flap bending moment response using estimated parameter values for the rotor model. For low Re, the elevon lift derivative was chosen as 75% of the theoretical value, $C_{l\delta} = 1.88/\text{rad}$, and the other aerodynamic parameter values used were: $C_{m\delta} = 0.34/\text{rad}$, $C_{l\alpha} = 6.28/\text{rad}$, and the value of K_α was adjusted to 6.0 to yield reasonable

results. These results are included in Fig 22 and confirm the experimentally observed behavior.

The phenomenon of “elevon reversal” has important implications for using trailing-edge on-blade elevon controls to replace the swashplate collective (0/rev) and cyclic (1/rev) blade root pitch for flight control. For example, the Kaman servo controlled rotor uses a torsionally flexible blade operating far above the “elevon reversal” rotor speed. (Torsionally stiff blade concepts dependent on the direct lift effect for rotor control have not been nearly as successful.) It should be noted, that at present, a principal barrier for using on-blade elevons for low frequency flight control is that the required blade pitch angles (15-20 deg) exceed the capability of smart material actuators.

With respect to the concept of active control for reducing rotor loads, vibration, and acoustics, all of which involve excitation frequencies at 3, 4, 5/rev or above, the “static” (and low frequency) elevon reversal characteristics are of less significance. At these higher frequencies, the complex aeroelastic structural dynamic responses of elastic bending and torsion modes are more dominant and will likely determine the effectiveness of the active control concept. (These characteristics will be discussed in more detail in later sections of the paper.) Alternatively, for enhancing rotor performance, where 0/rev and 2/rev excitation are of interest, the “elevon reversal” behavior may be of more significance.

Dynamic Response

Among the most fundamental characteristics of an active rotor system are the inherent or open loop dynamic response characteristics of the actuator, elevon, and rotor blade electro-aeroelastic system. These characteristics were a principal area of interest for the present investigation. In this section the results of dynamic testing will be presented including representative examples for blade root flap bending, root chord bending, root torsion, and elevon deflection for both nonrotating and rotating conditions. The experimental measurements are presented without comparison to analytical predictions, in the interest of reporting the available results as early as possible. It is expected that analytical comparisons will be forthcoming.

At the outset, it might be noted that the presence of an aerodynamic control surface mounted on the blade *in the rotating system* provides a unique opportunity to study the aeroelastic and structural dynamic characteristics of a rotor blade, as will be evident from the results to be presented here.

Dynamic response characteristics were primarily determined using a highly effective testing technique described earlier. Elevon actuator input voltage excitations were continuous logarithmic sine sweep signals and the measured elevon deflection and blade response output was analyzed with frequency response tools contained in the CIPHER[®] (Comprehensive Identification from FrEQuency Responses) software, Refs 25 and 26. This post processing generated frequency response functions of the input-output parameters. These included all the blade instrumentation parameters including PZT voltage, elevon deflection, and blade root flap bending, chord bending, and torsion moments. In addition to generating amplitude and phase of the frequency response functions, the CIPHER[®] technique also calculates a coherence function that permits judgments to be made regarding the validity of the identified frequency response.

Examples of the sine sweep excitation input and corresponding output responses in the time domain are given in Fig 23 for the nonrotating condition. The frequency varies from 1 Hz to 105 Hz in 27 seconds. The responses of the flap bending and torsion moment exhibit resonances as the input excitation sweeps across the bending and torsion mode frequencies.

Nonrotating, 0 RPM

All dynamic response data are presented for blade averaged data as described earlier, except where otherwise noted. In the case of elevon angle response, however, dynamic response results are always presented for blade 2.

Frequency response results are first presented for the nonrotating rotor blades at 3.5 deg collective pitch. Figure 24 shows the magnitude of the frequency response functions (FRFs) of blade root flap bending, chord bending, and torsion moment to elevon deflection input, and the FRF of elevon deflection to PZT voltage input. Moments were measured at the blade root, $r/R = 0.114$ for flap and chord bending and $r/R = 0.128$ for torsion moment. The measurements from the two blades were combined to give the average response (the collective, or symmetric, rotor mode for a two bladed rotor). Averaging the measurements reduces some of the antisymmetric noise sources and small fixed system interactions, and averages the effects of blade differences. It may be noted that the collective rotor mode uncouples the rotor from the fixed system for all force and moment components except the coupling of chordwise bending with rotor shaft torque.

The nonrotating FRF magnitudes are presented in dB (20 log magnitude) in Fig 24 in order to show the

responses of all the measurements on a single plot and permit the principal natural frequencies and structural dynamic couplings to be more clearly observed. The results are of high quality (low noise) as expected without aerodynamic damping and very low structural damping. Note that without elevon aerodynamic lift and pitch moment, the nonrotating excitation input consists of inertial excitation of the PZT beam mass, and the mass and inertia of the elevon and lever arm. The system natural frequencies/modes for flap, torsion, elevon, and chordwise modes are marked on the figures.

The blade 2 elevon deflection response to voltage excitation gives evidence of a natural mode at a frequency of about 78 Hz and is moderately damped as discussed earlier. The flap bending moment shows clear evidence of the first three flap bending modes, with quite low damping resulting in sharp peak responses. The cause of the evident truncation in the peak magnitude of the second flap bending mode is unknown. The larger response at the third flap mode relative to the second flap mode may be due to the elevon location closer to a node of second mode or an anti-node of third mode. Since blade mode shapes were not measured and analytical calculations have not been completed, more detailed interpretations are not possible at present.

The torsion mode response is clearly evident in the root torsion moment and shows the natural frequency near 56 Hz. Since the mass of the PZT bender beam is located behind the blade elastic axis, inertial forces and moments act to couple torsion and flap bending responses and small interactions in the torsion response are apparent at the flap bending mode frequencies.

The chordwise response is not of great importance here, but is included for completeness. Because the blade is at low pitch angle, untwisted, and the excitation is normal to the chordwise direction, the measured response is not of high accuracy. Nevertheless, the first chord mode is barely evident, and there is an interesting forced response by the torsion mode at the torsion natural frequency. Here the chordwise moment is excited by torsion motion through the bending-torsion coupling of the cantilever blade resulting from the elastic droop from gravity force. Smaller interactions are also evident at flap bending mode frequencies.

Rotating, 760 RPM

Frequency response measurements for the rotor operating at 760 RPM and 3.5 deg collective pitch are now discussed.

The magnitude of the frequency response functions (FRF) of 1) flap bending moment, 2) torsion moment to elevon deflection input, and 3) elevon deflection to PZT voltage input are shown in Fig 25. Here it is more useful to present the FRF magnitude on a linear scale. Again, the responses of the two blades are summed and averaged to filter out residual asymmetric n/rev periodic noise of the test environment and average the effects of blade dissimilarities (except that blade 2 is used for elevon angle data). Compared to the nonrotating results in Fig 24, the 760 RPM results are strongly influenced by structural dynamic and aerodynamic effects, as is evident in changes in natural frequencies, damping, and aerodynamic lift and moment of the elevon.

Principal noteworthy characteristics of the flap bending moment FRF are the resonant peaks at the second and third flap bending modes and a near absence of n/rev noise response except at the 1 and 2/rev frequencies. At 760 RPM, the second flap mode response is larger than the third mode. Interestingly, there is no peak flap bending response at torsion mode resonance as might be expected given the large increase in torsion moment (and presumably the blade angle of attack from elastic twist) but even without a distinct peak in flap bending moment, the effect of torsion may still be important. Further interpretation of this behavior will require comparisons with analytical predictions. It may also be noted again that strain gage measurements were taken only at the blade root, therefore, response variations along the blade span, that may influence the behavior of the blade root response, cannot be observed.

It may be noted that, for the in-phase (collective) elevon inputs, dynamic inflow and wake effects on blade lift and flap bending moment will be present only at even n/rev excitation frequencies, but that these effects should not be large due to operation at a non-zero thrust condition (3.5 deg collective pitch).

The torsion response to elevon deflection in Fig 25 exhibits expected behavior, peaking at the torsion mode natural frequency and showing aeroelastic coupling with the second and third flap bending modes. Finally, the elevon response shown in Fig 25 is substantially reduced in comparison to the nonrotating results, particularly in that the resonant response near 78 Hz is entirely suppressed by aerodynamic damping.

The phase and coherence of the flap bending and torsion moment FRFs are shown in Fig 26 and Fig 27.

Both phase plots show 180 deg phase shifts that coincide with the physical resonances visible in the corresponding magnitude of the flap bending moment and torsion moment FRFs of the previous figure. The initial torsion phase of -180 deg reflects the sign convention for elevon and torsion deflections, that is, elevon angle is positive for a downward deflection, torsion is positive nose up and thus a positive elevon angle produces a negative torsion moment for the steady state condition. The phase of the flap bending moment is only shown for frequencies of 30 Hz and above because of the low coherence for smaller frequencies. The coherence plot provides a measure of the accuracy and linearity of the FRFs (Ref. 25); a larger coherence indicates more reliable results. As previously noted, the n/rev noise present in the test environment contaminates the FRFs; this contamination is indicated by large reductions in the coherence at the n/rev frequencies. It may also be noted that the coherence for the torsion moment is, in general, significantly better than that for the flap bending moment.

A few results will now be presented to illustrate the extent to which the FRFs of the individual blades differ from one another. Figures 28 and 29 present the magnitude of flap bending and torsion moment FRFs of both blades for the 760 RPM, 3.5 deg collective pitch operating condition. The basic character of the responses is very similar, although there are significant differences in magnitude and phase of the two blades. Note that excitation of n/rev periodic noise is considerably more prominent in these FRFs than when the measurements for the two blades are averaged.

Rotating, RPM Varies

A useful way to better understand the dynamic response characteristics of the blade to elevon excitation is to observe the evolution of the frequency response functions (FRFs) as the rotor speed varies from zero to the nominal RPM. Several figures are presented for this purpose combining results for four different rotor speeds from 0 to 760 RPM.

First, Fig 30 shows the FRF magnitude of PZT current to PZT voltage for the elevon actuator of blade 2. As previously discussed, this electrical admittance (mA/V) at 0 RPM is not a linear function of frequency as a pure capacitor would be. In fact, the local minimum reveals the electromechanical coupling of this piezoceramic material. The effect of aerodynamic loading is to diminish the elevon-actuator mode resonant response and this appears as a linearization of the FRF as rotor speed increases. There is evidence of an increase in the frequency of this mode between 0

and 200 RPM as would be expected from the increasing elevon aerodynamic stiffness.

Figure 31 shows the FRF magnitude of elevon deflection to PZT voltage for blade 2. As previously discussed, the elevon dynamic response at 0 RPM strongly reflects the mechanical dynamics of the system and reveals a resonant response peak at about 80 Hz. In addition, the strong effect of aerodynamic loads is clear in the damped peak response of the actuator-elevon mode for higher rotor speeds. The reduction of steady state elevon deflection response is also clear and reflects the same effect shown in Fig 16 in the earlier section on actuator effectiveness.

The FRF magnitude of torsion moment to elevon deflection is shown Fig 32 for the same four rotor speeds. Again, the main features are clear: the steady state elevon effectiveness at low frequencies (as in Fig 20), the near invariance of torsion mode frequency with rotor speed, and the interactions with the second and third flap bending modes as marked on the figure.

It is of interest to infer the relative influence of the two primary sources of excitation of the root torsion moment, the aerodynamic pitching moment of the elevon and the inertial pitching moment of the PZT beam and elevon. If the reduction of unsteady aerodynamic moment with frequency were neglected, i.e., the aerodynamic excitation was assumed constant, then the torsion response at any rotor speed would largely be that of a damped, single degree of freedom, second order system. At first glance, it appears that the peak response at 760 RPM is simply the peak at 0 RPM plus the steady state response at 760 RPM. This occurrence is deceptive, however, since the aerodynamic damping at 760 RPM is substantially higher than the structural damping at 0 RPM. In fact, it appears that at 760 RPM the majority of the peak response is caused by the aerodynamic excitation of the elevon.

The FRF magnitude of flap bending moment to elevon deflection is shown in Fig 33. As would be expected, the effects of rotor speed and aerodynamics are very strong. Aerodynamics is particularly important for the second flap bending mode, as the resonant peak increases roughly by a factor of 20 from zero to 760 RPM. The third flap bending mode is not nearly as sensitive. Again it must be noted that the measurement is the root bending moment and the effect of the elevon on different modes will vary along the blade radius depending on the bending mode shapes and the elevon radial location.

These results further illustrate that the effectiveness of active elevon control for loads and vibration reduction will depend strongly on the

specific dynamic properties of the rotor blade at the important excitation frequencies present in forward flight. Additional analysis (particularly of the FRF phase measurements) will be needed to determine the relative importance, to the response, of the elevon lift effect and the torsion effect.

The behavior of the first flap bending mode in Fig 33 is unusual in that the responses for the 200 and 425 RPM rotor speeds are proportional to elevon excitation frequency up to about the first flap mode frequency. This is contrary to the expectation that the response should be relatively independent of excitation frequency at low frequencies as, for example, the 0 - 20 Hz torsion moment behavior in Fig 32. Note that at 760 RPM, the low frequency flap bending moment has nearly vanished due to the onset of elevon reversal (as in Fig 22).

Design Implications

The preliminary interpretations of the results presented above lead to observations that may be of use for future practical application of on-blade elevon control to reduce rotor vibratory loads. It should be noted that further understanding of the interplay of these dynamic response characteristics will benefit from additional analytical and experimental investigation.

The effectiveness of the elevon and the mechanism by which vibratory loads are reduced depend on the mode in which the elevon operates, and the number of elevons provided per blade. In the "torsion mode" the elevon generates elastic twist of the blade as the elevon aerodynamic pitch moment overcomes the blade torsional rigidity. In this case, the elevon is analogous to blade root pitch HHC/IBC. However, for practical values of blade torsional rigidity, useful elastic twist is likely to be produced only if the pitch moment acts in one direction along a majority of the blade span, and thus spanwise reversals in elastic twist that would be generated by multiple elevons are unlikely to be feasible. This implies that if on-blade elevons are operated in the "torsion mode", only a single control variable per blade would be available. Applied in the "torsion mode," the elevon effectiveness will increase when operated near the torsion natural frequency. Since the modes of interest for vibratory loads reduction will likely be the flap bending modes (2nd, 3rd, etc.) and their response at 3, 4, 5/rev, it may be desirable to design the blade torsion natural frequency in this region.

For the other mode of operation, termed a "lift mode," the elevon would alter the blade airload directly through elevon lift generated from $c_{l\delta}$. Although the associated torsion response influences

the lift significantly at low frequencies, at higher excitation frequencies this effect may be lessened since the torsion inertia increases the "effective torsional rigidity" of the blade. In the "lift mode" it is not important that the elevon produce the same effect along the blade, therefore, multiple elevons located at several spanwise locations may operate in different directions at the same time in order to control several flap bending modes independently. For operation in the lift mode rather than the torsion mode, the torsion frequency should be much less a determining factor for the vibration reduction of an active elevon system.

Of course, for a particular rotor system, the response and effectiveness of an active elevon system would exhibit some characteristics of each of these idealized behaviors. On the other hand, however, decisions on specific design variables such as number and location of elevons and modal frequency placement will depend on the particular modality of operation.

Concluding Remarks

A small scale model rotor was successfully tested in hover to explore the basic aeroelastic and structural dynamic characteristics of a rotor blade equipped with a 10% chord elevon control surface envisioned for eventual use as a means to attenuate rotorcraft vibratory loads. The principal findings are summarized as follows.

1. Demonstrated the practical feasibility of using piezoceramic bimorph actuators to provide reasonable elevon deflections for a small scale low tip speed model. Elevon deflections in excess of ± 10 deg and ± 5 deg were achieved at zero and the nominal 760 RPM rotor speed respectively.
2. Measured elevon deflection amplitude decreased with rotor speed in a manner consistent with the increase in aerodynamic hinge moment due to dynamic pressure.
3. Low-frequency blade torsion moment response to elevon deflection increased with rotor speed as expected. Elevon effectiveness, however, was lower than predicted by thin airfoil theory, largely due to the effects of low Reynolds number on elevon control power, $c_{m\delta}$.
4. Low frequency blade root bending response to elevon deflection increased due to elevon direct lift as rotor speed increases but then decreased due to the opposing effects of blade torsion induced by the negative aerodynamic pitching moment of the elevon, leading toward "elevon reversal" slightly above 760 RPM.

5. Continuous sine sweep frequency excitation proved to be an efficient experimental technique for measuring rotor blade frequency response characteristics when combined with the CIPHER[®] analysis system for post processing data analysis. This technique should be applicable for broader application to rotorcraft aeroelasticity and structural dynamics.

6. Frequency response measurements indicated that blade root torsion increased in conventional fashion to peak at the torsion natural frequency of about 60 Hz (4.7/rev) at 760 RPM. At resonance, torsion moment response was amplified approximately five times the steady state amplitude.

7. Blade root flap bending moment frequency response measurements clearly showed the large dynamic amplification due to elevon excitation at near the 2nd and 3rd flap bending mode frequencies.

8. The magnitude of the blade root flap bending responses produced by the available range of elevon deflection suggest that it will be possible to demonstrate significant reductions of the 3, 4, and 5/rev vibratory bending moments in forward flight in future tests.

9. Significant differences in the elevon performance, and torsion and bending moment responses between the two blades was observed in the measured results. These effects are not unexpected given the difficulty of building very precise small scale dynamic rotor blade models, particularly with the even smaller size of trailing edge elevons. These blade-to-blade differences, however, did not significantly impact the results obtained from this exploratory investigations.

Acknowledgments

The authors would like to thank Mr. David L. Sharpe for engineering guidance and assistance in preparing and conducting the hover test. They would also like to acknowledge the significant contributions of the entire test team. Finally, the authors gratefully acknowledge the outstanding effort of Mr. Terry L. Fish in fabricating the active elevon blades.

References

1. McHugh, F.J., and Shaw, J., Jr., "Benefits of Higher-Harmonic Blade Pitch: Vibration Reduction, Blade Load Reduction, and Performance Improvement," *American Helicopter Society Mideast Region Symposium on Rotor Technology*, Essington, PA, August 11-13, 1976.
2. Miao, W., Kottapalli, S.B.R., and Frye, H.M., "Flight Demonstration of Higher Harmonic Control (HHC) on S-76," *Proceedings of the 42nd Annual Forum of the*

American Helicopter Society, Washington, DC, June 2-4, 1986, pp. 777-791.

3. Yu, Y.H., Gmelin, B., Heller, H., Philippe, J.J., Preisser, J.S., "HHC Aeroacoustic Rotor Test at the DNW - The Joint German/French/US Project," *Proceedings 20th European Rotorcraft Forum*, Amsterdam, The Netherlands, 1994.

4. Jacklin, S.A., Blass, A., Swanson, S.M., and Teves, D., "Second Test of a Helicopter Individual Blade Control System in the NASA Ames 40- by 80-Foot Wind Tunnel," *Proceedings American Helicopter Society 2nd International Aeromechanics Specialists' Conference*, Bridgeport, Connecticut, October 11-13, 1995.

5. Strehlow, H., and Rapp, H., "Smart Materials for Helicopter Rotor Active Control," Paper No. 5, *Presented at the AGARD/SMP Specialist's Meeting on Smart Structures for Aircraft and Spacecraft*, Lindau, Germany, October 5-7, 1992.

6. Chopra, I., "State-of-the-Art of Smart Structures and Integrated Systems," *SPIE Smart Structures and Materials Conference*, San Diego, CA, February 25-29, 1996.

7. Crawley, E.F., and de Luis, J., "Use of Piezoelectric Actuators as Elements of Intelligent Structures," *AIAA Journal*, Vol. 25, No. 10, October, 1987.

8. Loewy, R.G., "Recent Developments in Smart Structures with Aeronautical Applications," *37th Israel Annual Conference on Aerospace Sciences*, Tel Aviv, Haifa, Israel, February 26-27, 1997.

9. McCloud, J.L., III, and Weisbrich, A.L., "Wind Tunnel Test Results of a Full Scale Multi-cyclic Controllable Twist Rotor," *Proceedings of the 34th Annual National Forum of the American Helicopter Society*, Washington, DC, May 15-17, 1978.

10. Ormiston, R.A., "Can Smart Materials Make Helicopters Better?," *Presented at the Fourth Workshop on Dynamics and Aeroelastic Stability Modeling of Rotorcraft Systems*, College Park, Maryland, November 19-21, 1991.

11. Millott, T.A., and Friedmann, P.P., "Vibration Reduction in Helicopter Rotors Using an Active Control Surface Located on the Blade," *AIAA-92-2451-CP, Proceedings 33rd AIAA/ASME/ASCE/ AHS/ASC Structures, Structural Dynamics, and Materials Conference*, Dallas, TX, April 13-15, 1992, pp 1975-1988.

12. Millott, T.A., and Friedmann, P.P., "Vibration Reduction in Helicopter Rotors Using an Actively Controlled Partial Span Trailing Edge Flap Located on the Blade," *NASA CR 4611*, June 1994.

13. Milgram, and Chopra, I., "Helicopter Vibration Reduction with Trailing Edge Flaps," *Proceedings of the American Helicopter Society Northeast Region*

Aeromechanics Specialists' Meeting, Stratford, Connecticut, October, 1995.

14. Straub, F.K., and Charles, B.D., "Preliminary Assessment of Advanced Rotor/Control System Concepts (ARCS)," USA AVSCOM TR 90-D03, 1990.

15. Fenn, R.C., Downer, J.R., Bushko, D.A., Gondhalekar, V., and Ham, N.D., "Terfenol-D Driven Flaps for Helicopter Rotor Vibration Reduction," *Smart Materials & Structures*, Vol. 5, No. 1, 1996, pp. 49-57.

16. Straub, F.K., "A Feasibility Study of Using Smart Materials for Rotor Control," *Smart Materials and Structures*, Vol. 5, No. 1, February, 1996.

17. Spangler, R.L., and Hall, S.R., "Piezoelectric Actuators for Helicopter Rotor Control," Paper No. 90-1076-CP, *Proceedings of the 31st Structures, Structural Dynamics and Materials Conference*, Long Beach, California, April 2-4, 1990.

18. Chen, P.C., Samak, D.K., and Chopra, I., "Development of an Intelligent Rotor," *Presented at the Fourth Workshop on Dynamics and Aeroelastic Stability Modeling of Rotorcraft Systems*, College Park, Maryland, November 19-21, 1991.

19. Samak, D.K., and Chopra, I., "A Feasibility Study to Build a Smart Rotor: Trailing Edge Flap Actuation," *Presented at SPIE's 1993 Conference on Smart Structures and Materials*, Albuquerque, New Mexico, February, 1993.

20. Walz, C., and Chopra, I., "Design and Testing of a Helicopter Rotor Model with Smart Trailing Edge Flaps," Paper No. 94-1767-CP, *Proceedings of the 35th Structures, Structural Dynamics and Materials Conference, Adaptive Structures Forum*, Hilton Head, South Carolina, April 18 -- 20, 1994.

21. Ben-Zeev, O., and Chopra, I., "Advances in the Development of an Intelligent Helicopter Rotor Employing Smart Trailing-Edge Flaps," *Smart Materials & Structures*, Vol. 5, No. 1, 1996.

22. Fulton, M.V., "Development of a Small-Scale Rotor with On-Blade Elevons," *Presented at the Second Workshop on Smart Structures and Materials*, College Park, Maryland, September 5-7, 1995.

23. Maier, T.H., Sharpe, D.L., and Lim, J.W., "Fundamental Investigation of Hingeless Rotor Aeroelastic Stability, Test Data and Correlation," *Presented at the American Helicopter Society 51st Annual Forum*, Fort Worth, Texas, May 9-11, 1995.

24. Jacobs, E.N., and Pinkerton, R.N., "Pressure Distributions Over a Symmetrical Airfoil Section with Trailing Edge Flap," NACA Report No. 360, 1930.

25. Tischler, M.B., Cauffman, M.G., "Frequency-Response Method for Rotorcraft System Identification: Flight Applications to BO-105 Coupled

Rotor/Fuselage Dynamics," *Journal of the American Helicopter Society*, Vol. 37, No. 3, July 1992, pp. 3-17.

26. Tischler, M.B., Driscoll, J.T., Cauffman, M.G., and Freedman, C.J., "Study of Bearingless Main Rotor Dynamics from Frequency-Response Wind Tunnel Test Data," *Presented at the American Helicopter Conference*, San Francisco, CA, January 19-21, 1994.

27. Flint, E., Liang, C., and Rogers, C.A., "Electromechanical Analysis of Piezoelectric Stack Active Member Power Consumption," *Journal of Intelligent Material Systems and Structures*, Vol. 6, January, 1995, pp. 117-124.

Ideal Concept Possibilities

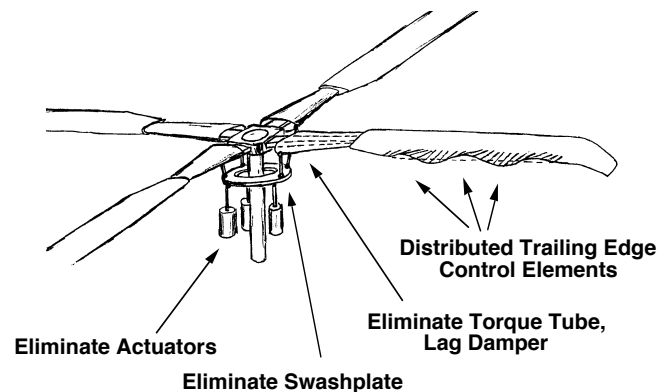


Fig. 1 Idealized active elevon concept for vibratory loads reduction and flight control function.

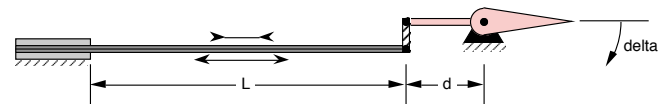


Fig. 2 Schematic of bimorph and elevon geometry, L = length of bimorph bender beam, d = elevon lever arm length.

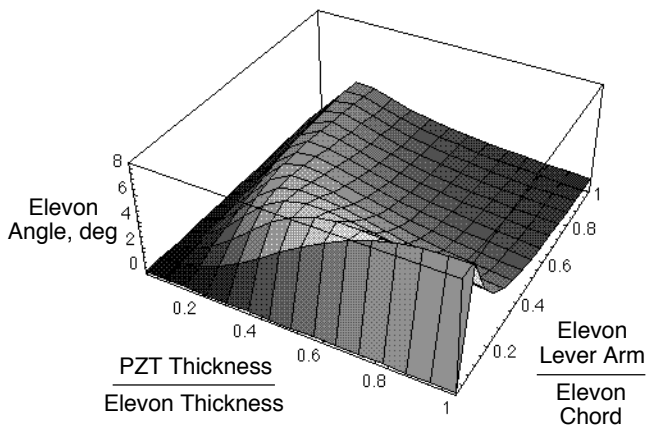


Fig. 3 Influence of PZT bimorph and elevon design variables for maximizing elevon response.

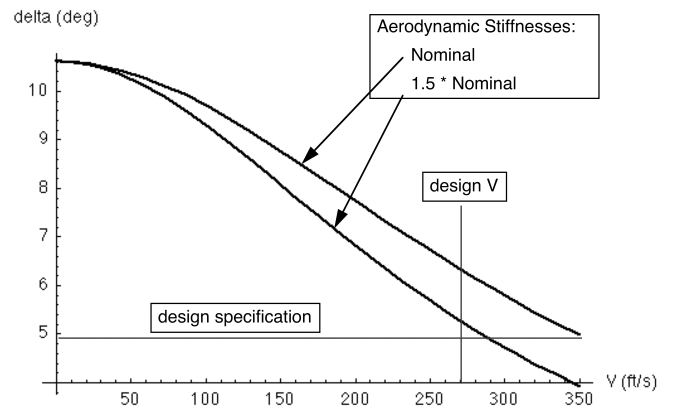


Fig. 5 Effect of airspeed on elevon deflection angle.

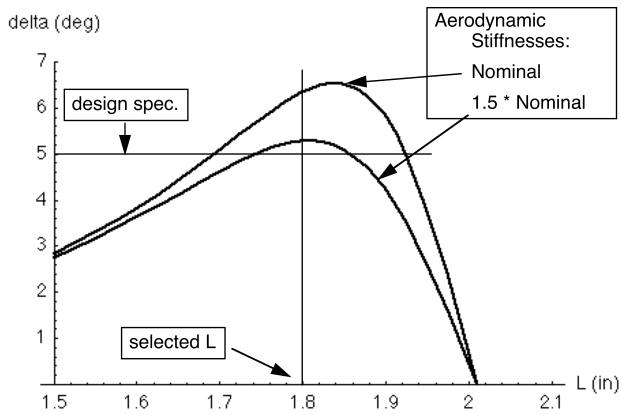


Fig. 4 Variation of elevon deflection with PZT bimorph length.

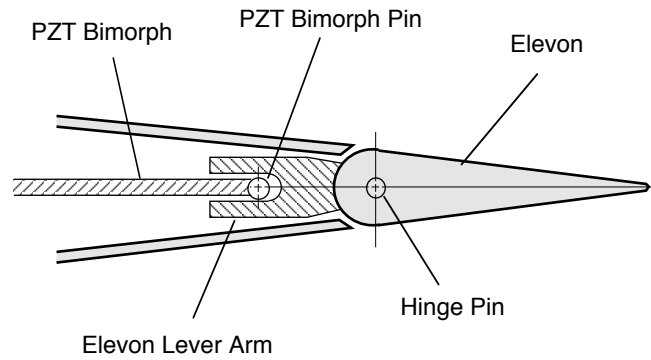


Fig. 6 Airfoil cross section, PZT bimorph bender beam and elevon lever arm mechanism.



Fig. 7 Blade planform showing fiberglass spar, active elevon section and PZT actuator layout.

Table 1. Rotor Characteristics & Operating Conditions.

Description	Variable	Value
No. of Blades	b	2
Rotor Radius	R	45 in (3.75 ft)
Airfoil		NACA 0012
Airfoil Chord	c	3.4 in
Elevon Chord	c_{elv}	0.34 in (10% c)
Elevon Span	S_{elv}	5.55 in (12% R)
Solidity	σ	0.048
Lock No.	γ	5 -- 7.5
Precone	β_o	0.0
Nominal Rotor Speed	Ω_o	760 RPM (12.7 Hz)
1st Flap Mode	$\omega_{\beta 1}$	1.11 / rev [*]
1st Lag Mode	$\omega_{\zeta 1}$	1.08 / rev [*]
1st Torsion Mode	$\omega_{\phi 1}$	4.6 / rev [*]
Airspeed	V_{tip}, V_{elv}	298, 224 ft/s
Dynamic Pressure	q_{tip}, q_{elv}	106, 60 lb/ft ²
Reynolds Number	Re_{tip}, Re_{elv}	540,000; 400,000
Mach Number	M_{tip}, M_{elv}	0.27, 0.20

* $\theta_0=0$ deg, 760 RPM, in air

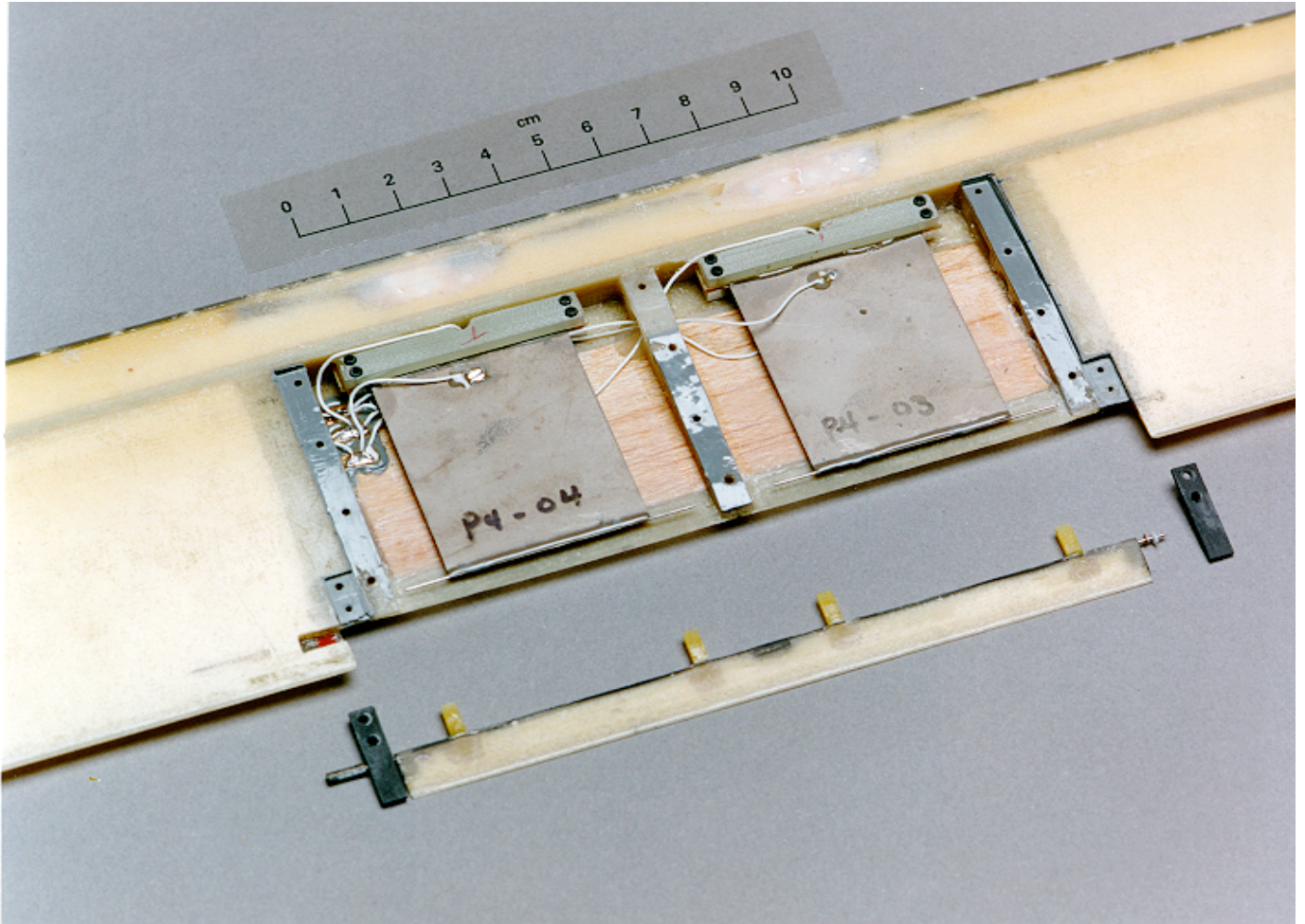


Fig. 8 Active elevon section of the blade with access panel removed and elevon and hinge pin bearing blocks disassembled.

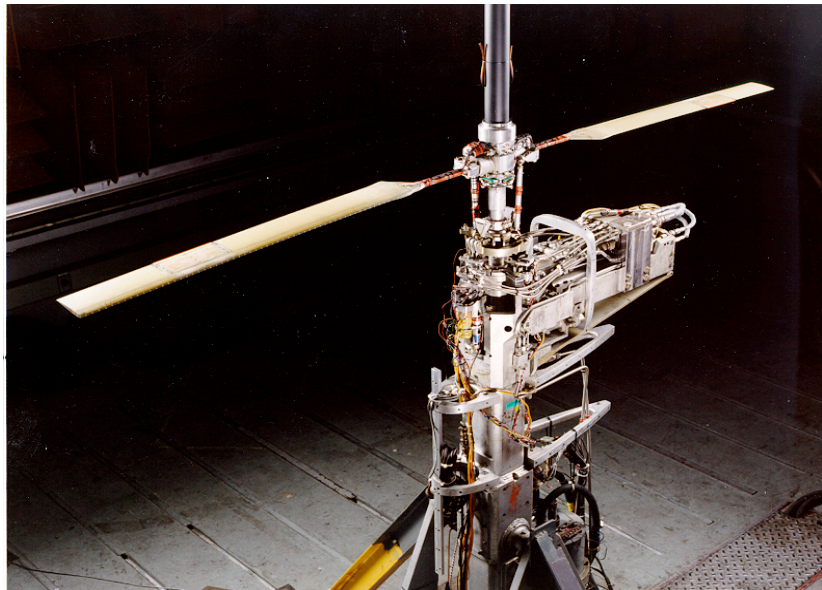


Fig. 9 Rotor installed on the Small Scale Rotor Test Rig in the U.S. Army Aeroflightdynamics Directorate Hover Test Chamber.

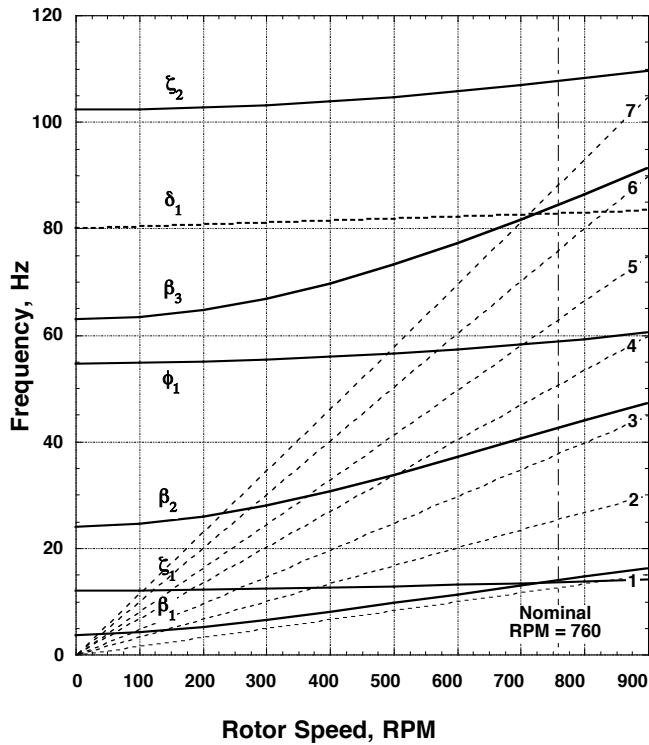


Fig. 10 Rotor blade frequencies versus rotor speed in air at zero collective pitch.

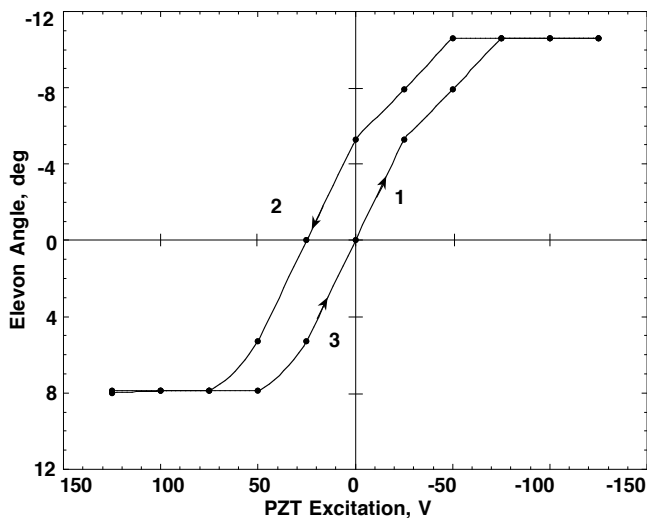


Fig. 11 Nonlinear static hysteresis characteristics of actuator-elevon deflection, blade 1.

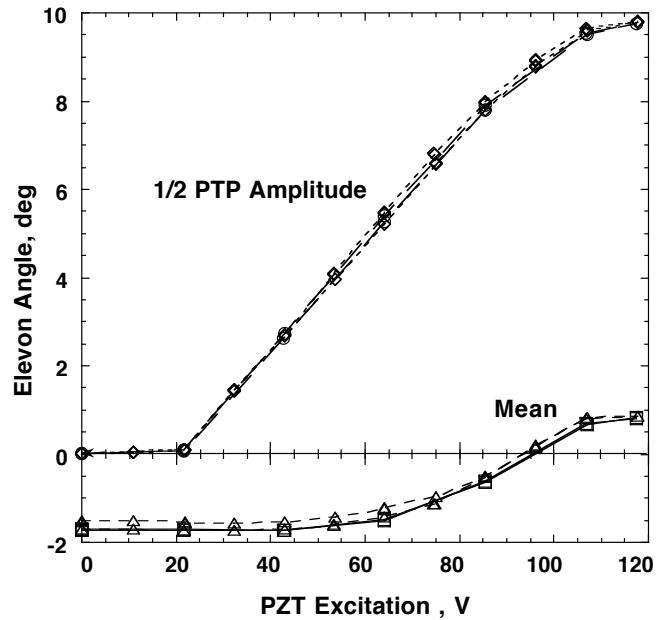


Fig. 12 Nonrotating amplitude and mean elevon deflection of blade 1 as a function of PZT bimorph excitation voltage, 5 Hz.

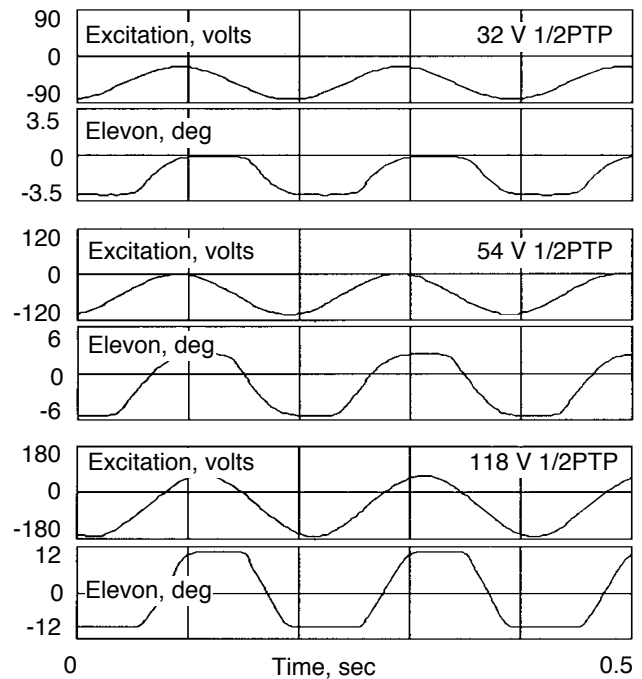


Fig. 13 Effect of excitation voltage level on nonlinear response of PZT bimorph actuator and elevon, 5 Hz, nonrotating, blade 1.

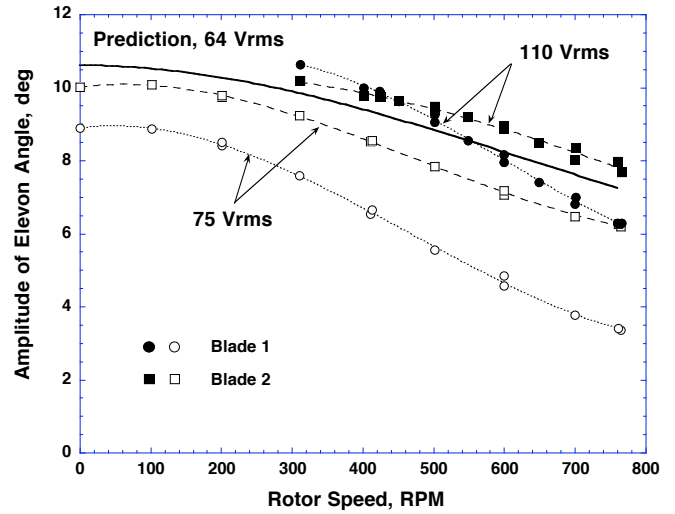


Fig. 16 Elevon actuator effectiveness, elevon deflection amplitude versus rotor speed, 5 Hz excitation, collective pitch $\theta_0 = 3.5$ deg.

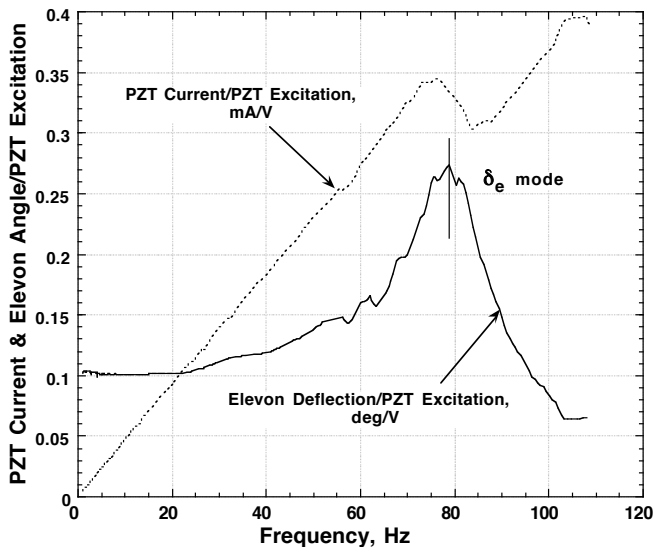


Fig. 15 Frequency response magnitude for elevon actuator current and elevon deflection to PZT excitation voltage, blade 2, nonrotating.

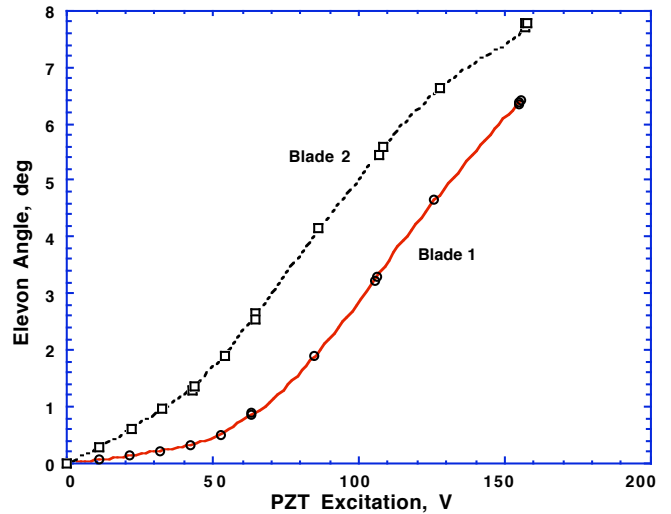


Fig. 17 Elevon deflection amplitude versus PZT excitation voltage, 760 RPM, 5 Hz, $\theta_0 = 3.5$ deg.

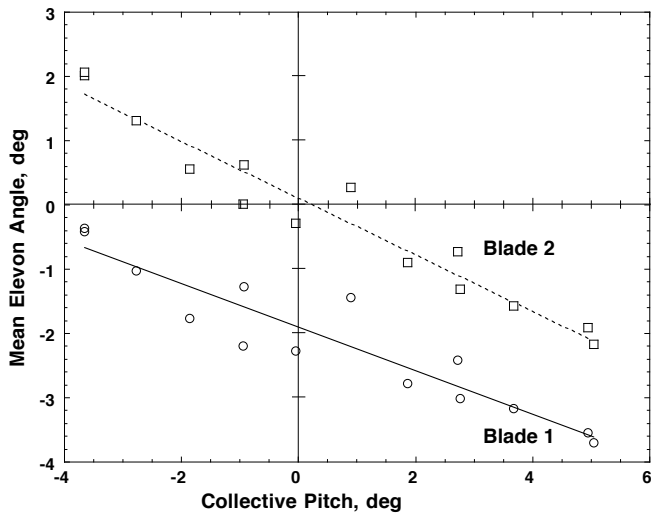


Fig. 18 Mean elevon deflection versus collective pitch, 760 RPM, 5 Hz, $V_{rms} = 30$ volts.

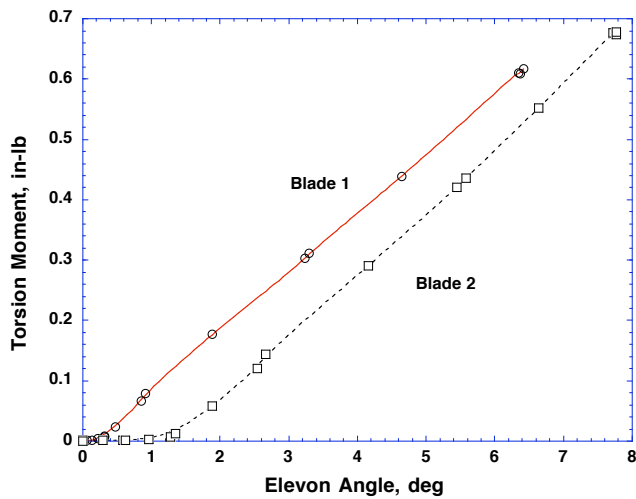


Fig. 19 Blade root torsion moment amplitude versus elevon deflection, 5 Hz, 760 RPM, $\theta_0 = 3.5$ deg.

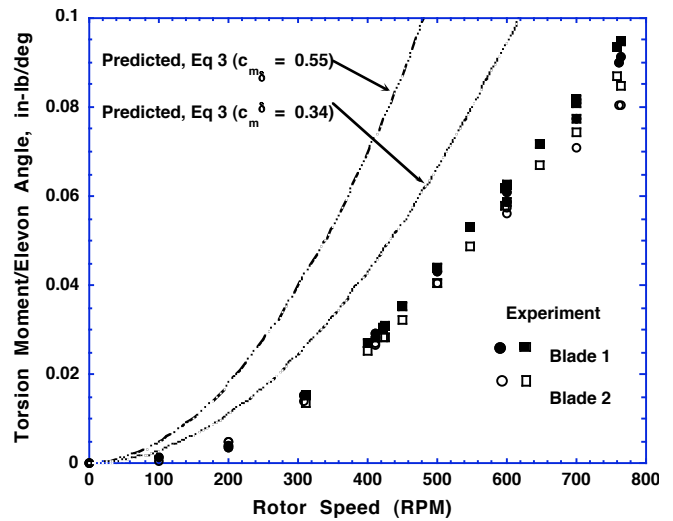


Fig. 20 Elevation torsion moment effectiveness versus rotor speed, 5 Hz, $\theta_0 = 3.5$ deg.

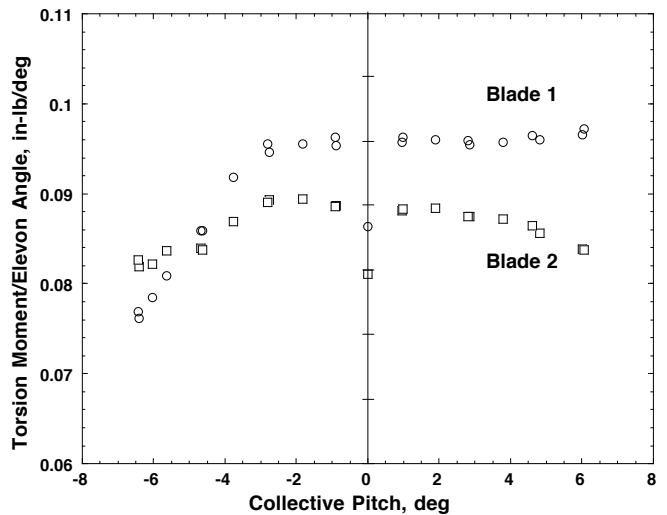


Fig. 21 Effect of collective pitch on elevation torsion moment effectiveness, 5 Hz, 760 RPM.

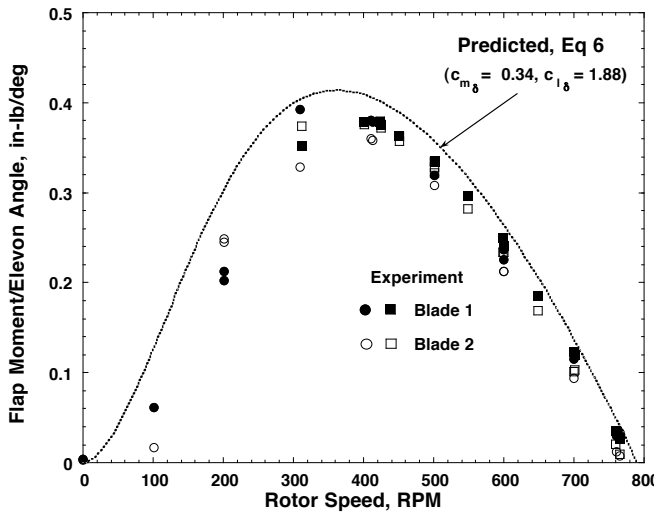


Fig. 22 Elevon flap bending moment effectiveness versus rotor speed, 5 Hz, $\theta_0 = 3.5$ deg - "elevon reversal" effect.

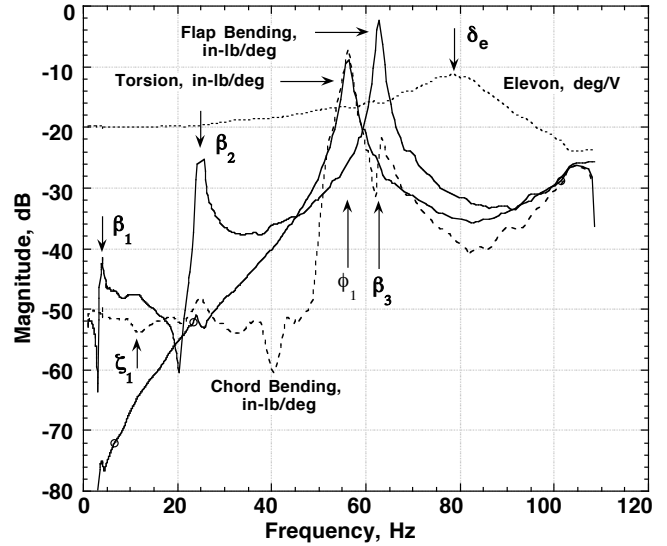


Fig. 24 Nonrotating frequency response function magnitudes, 2-blade average (except blade 2 for elevon response), $\theta_0 = 3.5$ deg.

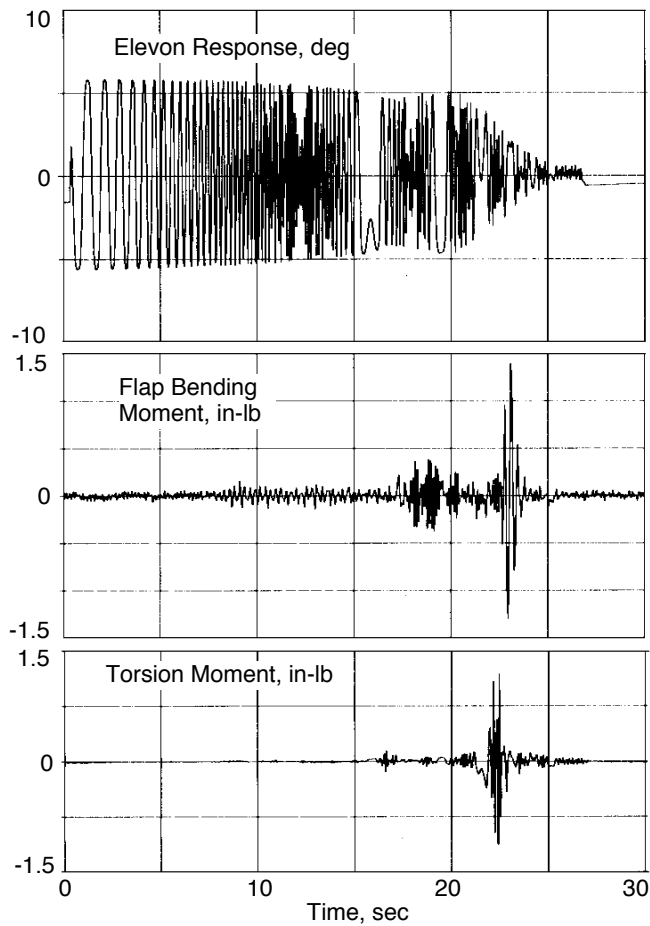


Fig. 23 Example of response to sine sweep excitation used with CIPHER[®] method for frequency response functions.

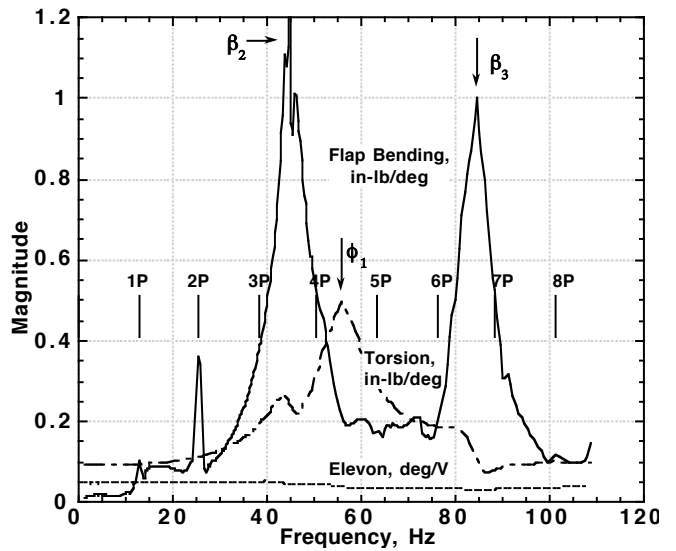


Fig. 25 Frequency response functions, 2-blade average (except blade 2 for elevon response), RPM = 760, $\theta_0 = 3.5$ deg.

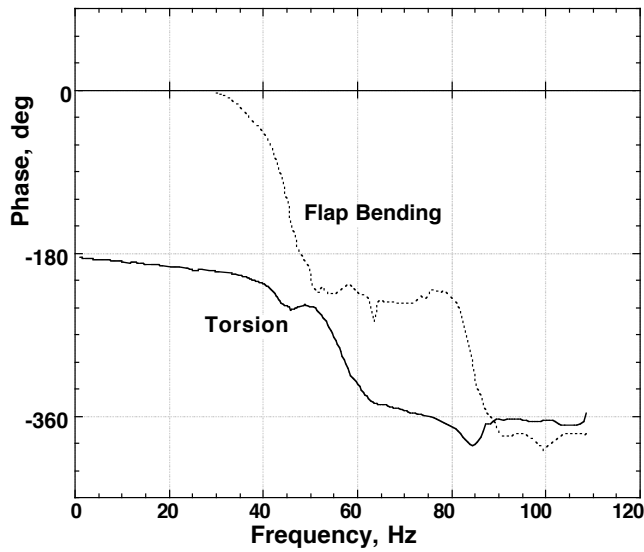


Fig. 26 Phase of frequency response functions for flap bending and torsion moments, 2-blade average, RPM = 760, $\theta_0 = 3.5$ deg.

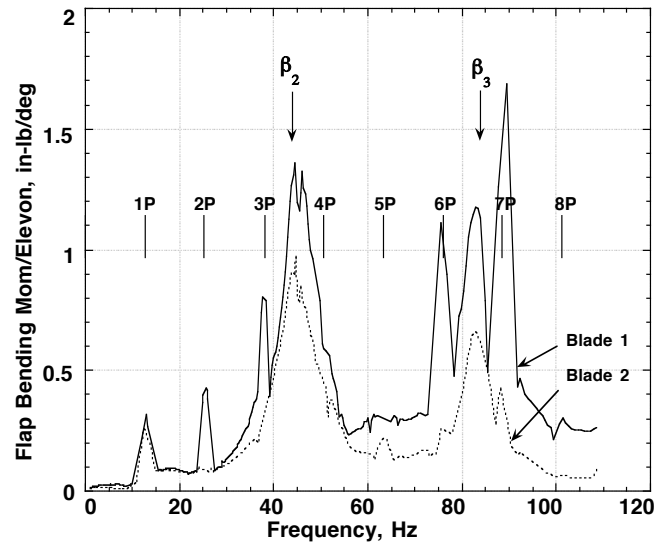


Fig. 28 Blade-to-blade variation in flap bending moment frequency response function magnitude, RPM = 760, $\theta_0 = 3.5$ deg.

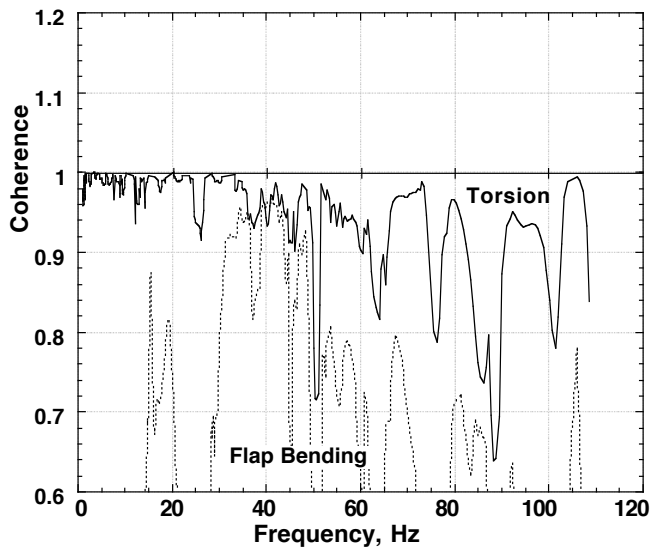


Fig. 27 Coherence of frequency response functions for flap bending and torsion moments, 2-blade average, RPM = 760, $\theta_0 = 3.5$ deg.

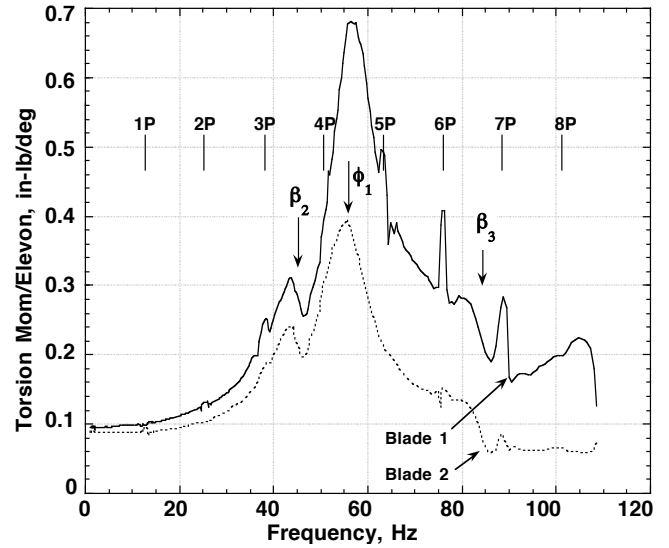


Fig. 29 Blade-to-blade variation in blade root torsion moment frequency response function magnitude, RPM = 760, $\theta_0 = 3.5$ deg.

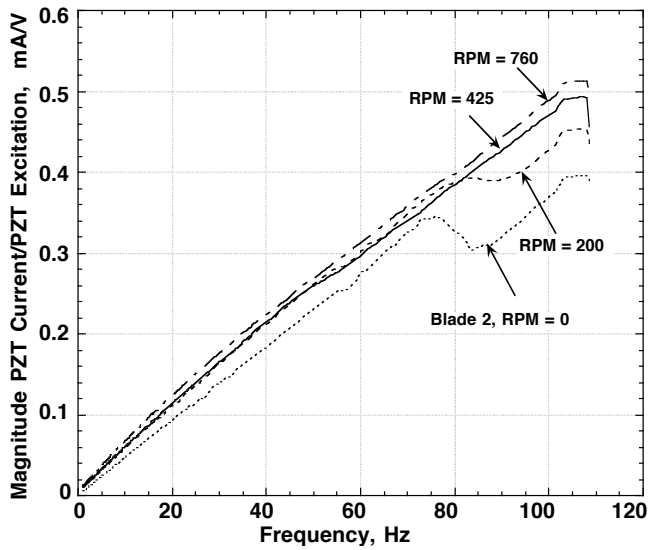


Fig. 30 Variation with rotor speed of PZT current (blade 2) frequency response, $\theta_0 = 3.5$ deg (except $\theta_0 = 0$ deg for 0 RPM).

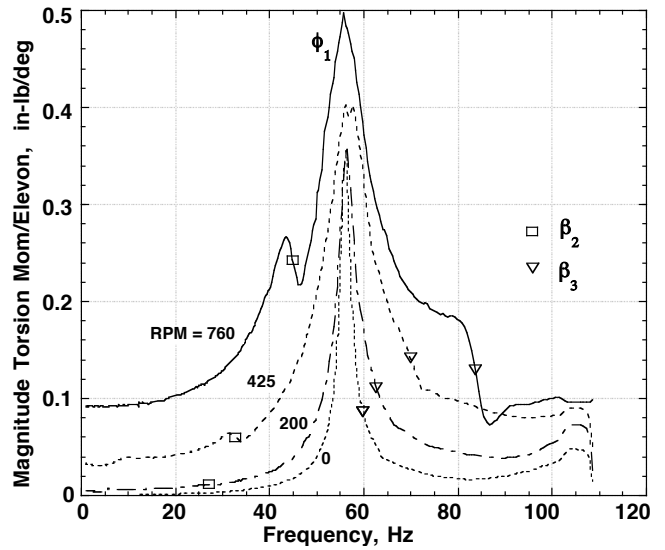


Fig. 32 Variation with rotor speed of blade root torsion moment frequency response (2-blade average), $\theta_0 = 3.5$ deg.

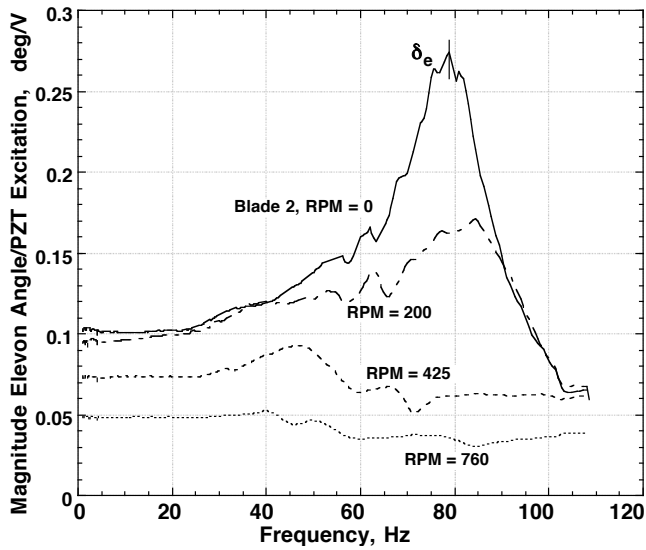


Fig. 31 Variation with rotor speed of elevon deflection (blade 2) frequency response, $\theta_0 = 3.5$ deg.

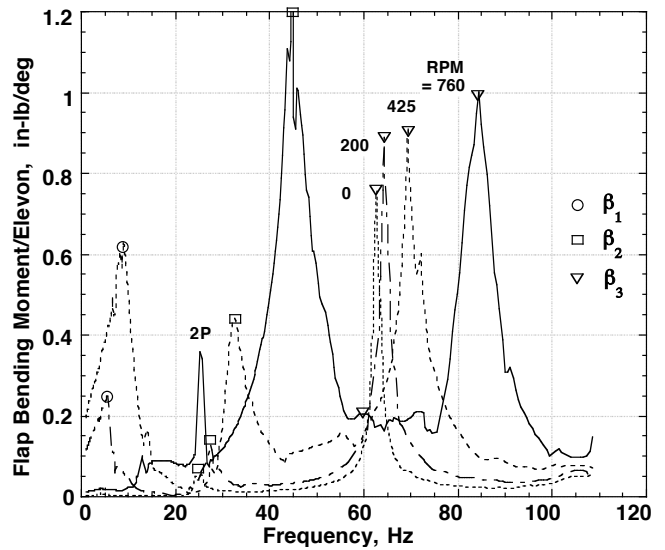


Fig. 33 Variation with rotor speed of blade root flap bending moment frequency response (2-blade average), $\theta_0 = 3.5$ deg.